Hindawi
Wireless Communications and Mobile Computing
Volume 2019, Article ID 9249352, 13 pages
https://doi.org/10.1155/2019/9249352

Research Article

Broadside-Coupled Microstrip Lines as Low Loss Metamaterial for Microwave Circuit Design

Shaofang Gong[1], **Xin Xu**[2] **and Magnus Karlsson**[1]

[1]*Department of Science and Technology, Linköping University, Norrköping, Sweden*
[2]*School of Electronic Science and Engineering, University of Electronic Science and Technology of China, Chengdu, China*

Correspondence should be addressed to Shaofang Gong; shaofang.gong@liu.se

Received 8 February 2019; Accepted 7 April 2019; Published 4 July 2019

Academic Editor: Eva Antonino-Daviu

The entire microwave theory is based on Maxwell's equations, whereas the entire electronic circuit theory is based on Kirchhoff's electrical current and voltage laws. In this paper, we show that the traditional microwave design methodology can be simplified based on a broadside-coupled microstrip line as a low loss metamaterial. That is, Kirchhoff's laws are still valid in the microwave spectrum for narrowband signals around various designated frequencies. The invented low loss metamaterial has been theoretically analyzed, simulated, and experimentally verified in both time and frequency domains. It is shown that the phase velocity of a sinusoidal wave propagating on the low loss metamaterial can approach infinity, resulting in time-space shrink to a singularity as seen from the propagating wave perspective.

1. Introduction

Microwave theory and techniques, based on Maxwell's equations, and electronic circuit theory and techniques, based on Kirchhoff' electrical current and voltage laws, are traditionally two distinguishable disciplines in both university education and industrial research and development. It is known that Kirchhoff's electrical current and voltage laws can be derived from Maxwell's equations under a time-invariant or slowly changing field condition [1]. Therefore, to use Kirchhoff's laws in analog circuit design is truly valid at a relatively low frequency, e.g., below 300 MHz. At a higher frequency than 300 MHz, the so-called radio frequency (RF) design methodology has been utilized, which takes the inaccuracy of Kirchhoff's laws into account. At a frequency of a few gigahertz and above, microwave theory and techniques are employed.

Now a challenging question is, can we find a way to accurately use Kirchhoff's laws in the microwave and even mm-wave spectrums? If the answer is yes, microwave designs that are difficult for many electronic engineers can be simplified. Moreover, new circuitry architectures and topologies may be worked out for future communication technologies. Theoretically, it is possible to converge Maxwell's equations and Kirchhoff's laws for microwave and even mm-wave circuit designs, as shown in the next section. The precondition is to let both permittivity (ε) and permeability (μ) be zero in Maxwell's equations.

Metamaterial has become a research interest since early 2000s, when its existence was experimentally verified with man-made structures [2–4], even though a theoretical concept of metamaterial had been published much earlier in the literature [5]. The properties of metamaterial are characterized by its negative and zero permittivity and/or permeability. These properties do not exist with material in nature, since the permittivity and the permeability of free-space are positive values, i.e., $\varepsilon_0 = 8.854 \times 10^{-12}$ F/m and $\mu_0 = 4\pi \times 10^{-7}$ H/m, whereas the permittivity and permeability values in a medium are larger than these values. To date, various metamaterial structures in one, two, and three dimensions have been proposed and studied [6–13]. However, previous published metamaterial structures have some common problems, e.g., high loss for electromagnetic wave propagation and difficulty in manufacturing metamaterial structures with precision at a high frequency.

Table 1: Unit dimensions.

f_0 (GHz)	w_a (mm)	l_a (mm)	w_b (mm)	l_b (mm)
1	3.67	9.80	0.25	12.3
2	3.67	4.67	0.25	7.05
3	3.67	3.20	0.25	4.46

In this paper we present a low loss metamaterial structure based on broadside-coupled microstrip lines, which avoids the aforementioned problems. Moreover, it is compatible with traditional transmission line design, e.g., microstrip lines on a planar structure. Based on this low loss metamaterial structure, a detailed study around the transition region from left- to right-handed wave propagations on the metamaterial has been done. It is shown that at various designated frequencies, the phase velocity of a sinusoidal wave approaches infinity, leading to time-space shrink to a singularity and resulting in zero permittivity and zero permeability of the metamaterial. Consequently, a simplified design methodology based on Kirchhoff's laws can be utilized for microwave circuitry analyses, when the low loss metamaterial is utilized at various designated frequencies above 1 GHz.

2. Model and Theory

We start from the first principle, i.e., from Maxwell's equations, and let both permittivity and permeability be zero, and then we study our proposed metamaterial structure with broadside-coupled microstrip lines.

2.1. Maxwell's Equations When Both ε and μ Are Zero. The four Maxwell's equations in differential form under the condition of null magnetic current source are described below [14].

$$\nabla \times \widehat{H} = \widehat{J} + \varepsilon \frac{\partial \widehat{E}}{\partial t}, \tag{1}$$

$$\nabla \times \widehat{E} = -\mu \frac{\partial \widehat{H}}{\partial t}, \tag{2}$$

$$\nabla \cdot \varepsilon \widehat{E} = \rho, \tag{3}$$

$$\nabla \cdot \mu \widehat{H} = 0, \tag{4}$$

where $\widehat{H}$ is the magnetic field intensity, $\widehat{E}$ the electric field intensity, ρ the electric charge density, ε permittivity of a medium, μ permeability of a medium, and t the time variable. From (1) and (2),

$$\nabla \times \widehat{H} = \widehat{J}, \quad \text{if } \varepsilon = \varepsilon_r \varepsilon_0 = 0, \tag{5}$$

$$\nabla \times \widehat{E} = 0, \quad \text{if } \mu = \mu_r \mu_0 = 0, \tag{6}$$

where ε_r is the relative permittivity (dielectric constant) and ε_0 the permittivity of free-space, whereas μ_r is the relative permeability and μ_0 the permeability of free-space. Using (5),

$$\nabla \cdot \widehat{J} = \nabla \cdot \left(\nabla \times \widehat{H}\right) \equiv 0, \tag{7}$$

which is equivalent to the following equation in the integral form according to the divergence theorem [14].

$$\iiint_v \nabla \cdot \widehat{J} dv = \oiint_s \widehat{J} \cdot d\widehat{s} = \sum_k I_k = 0 \quad \text{at a node,} \tag{8}$$

where I_k is an electrical current, flowing either in or out at a node.

Similarly, from (6) the following form can be obtained according to the Stokes' theorem [14]:

$$\iint_s \left(\nabla \times \widehat{E}\right) \cdot d\widehat{s} = \oint_c \widehat{E} \cdot d\widehat{l} = \sum_k V_k = 0 \quad \text{along a closed loop,} \tag{9}$$

where V_k is the electrical voltage between two points on a loop.

It is apparent that Kirchhoff's current law, i.e., (8), can be derived from Maxwell's equations under the precondition of $\varepsilon = \varepsilon_r \varepsilon_o = 0$. Similarly, Kirchhoff's voltage law, i.e., (9), is derived under the precondition of $\mu = \mu_r \mu_o = 0$. Note that (3) and (4) are not needed to obtain (8) and (9). However, from (3) $\rho = 0$ when $\varepsilon = \varepsilon_r \varepsilon_o = 0$, indicating no electric charge accumulation. When ε deviates from null, ρ becomes nonzero.

Note that in the above derivations, $\partial \widehat{E}/\partial t$ and $\partial \widehat{H}/\partial t$ in (1) and (2) can be nonzero, which means that the above derivations are valid under time-variant electrical and magnetic field conditions. This means that, when both ε and μ are zero, Kirchhoff's laws are valid not only under a static or slowly changing field condition as in the standard circuit theory for a direct current (dc) or an alternate current (ac) circuitry, but also under fast-changing field conditions as in a microwave or a mm-wave circuitry.

2.2. Broadside-Coupled Microstrip Line Model. Figures 1(a) and 1(b) show oblique-top and side views of our proposed metamaterial structure with two series broadside-coupled microstrip lines and one shunt short-circuit stub with multiple vias for good grounding. Figure 1(c) illustrates that two or more unit cells are cascaded. Dimensions of the structure designated for 1, 2, and 3 GHz are listed in Table 1. The substrate thickness is t_1 = 0.17 mm and t_2 = 1.52 mm, respectively. The substrate material used is Rogers RO4350B with a dielectric constant ε_r= 3.66 ± 0.05 and a loss factor of 0.0031 @ 2.5 GHz (0.0037 @ 10 GHz).

Figure 2(a) depicts a lossless equivalent model of the metamaterial unit cell shown in Figures 1(a) and 1(b), where C_p is a series capacitance of the broadside-coupled line segment, either to the left or to the right of the middle short-circuit stab having a shunt inductance of L_s. The shunt capacitance of the broadside-coupled line segment to ground is C_{pg}.

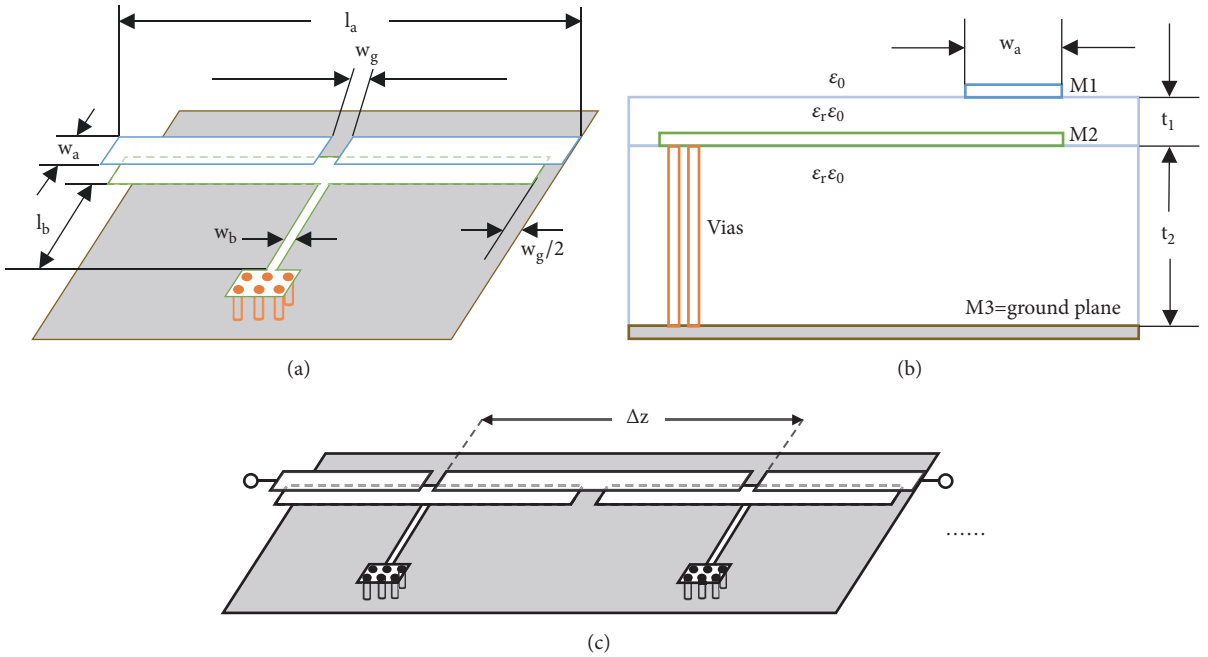

FIGURE 1: Metamaterial with broadside-coupled microstrip lines and short-circuit stubs with multiple vias. (a) Oblique-top view of a unit cell. (b) Side view of the unit cell. (c) Two or more unit cells are cascaded.

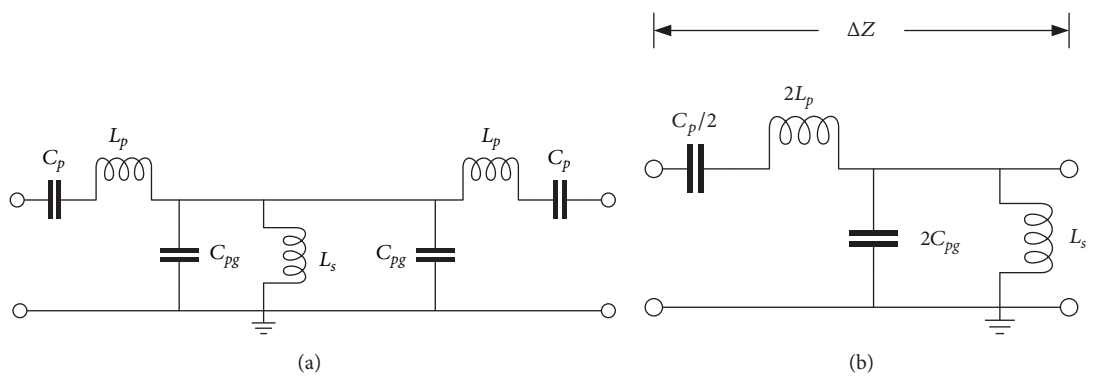

FIGURE 2: Lossless equivalent model of (a) the unit cell shown in Figure 1(a), and (b) the middle unit section marked with Δz shown in Figure 1(c).

To simplify this model for analysis, we can choose the middle unit section between two cascaded unit cells with a length of Δz, as illustrated in Figure 1(c). The equivalent model is then simplified to Figure 2(b). Apparently, Figure 2(b) shows a typical lossless metamaterial model with a composed left- and right-handed transmission line. In our case, we have used only microstrip lines to realize the metamaterial, avoiding any discrete capacitor or inductor, e.g., interdigital capacitor used in [4]. This can be an advantage, since the design of the metamaterial is then scalable with frequency, similar to traditional microwave circuit design using microstrip lines. Moreover, our previous study [15, 16] has shown that low loss and broadband properties can be achieved with broadside-coupled microstrip lines.

Using the model shown in Figure 2(b), the series impedance Z and shunt admittance Y of a unit section of Δz length are described below.

$$Z = j\left(\omega L'_R \Delta z - \frac{1}{\omega C_L}\right) = j\left(\omega L'_R - \frac{1}{\omega C_L \Delta z}\right)\Delta z, \quad (10)$$

$$Y = j\left(\omega C'_R \Delta z - \frac{1}{\omega L_L}\right) = j\left(\omega C'_R - \frac{1}{\omega L_L \Delta z}\right)\Delta z, \quad (11)$$

where $L'_R = 2L_p/\Delta z$ and $C'_R = 2C_{pg}/\Delta z$ are unit length series inductance and unit length shunt capacitance of the broadside-coupled line, whereas $C_L = C_p/2$ is the total series capacitance of the broadside-coupled line with a length of Δz. $L_L = L_S$ is the total shunt inductance of the short-circuit stub,

and $\omega = 2\pi f$ is an angular frequency, whereas f is a frequency. Note that in (10) and (11), we have used the total inductance and total capacitance for L_L and C_L, instead of unit length capacitance and unit length inductance. The reason is that, unlike L'_R and C'_R, L_L and C_L are not linearly scalable with Δz that is the minimum length of a metamaterial section at a designated frequency.

It should be pointed out that, in a conventional transmission line theory [17], Δz should be infinitesimally small. However, for the metamaterial structure shown in Figure 1, Δz, i.e., l_a in Figure 1(a), is dependent on the shunt stub length l_b. As seen in Table 1, when l_b = 12.3 mm, the unit cell length l_a = Δz = 9.80 mm at 1 GHz that has a wavelength λ of 300 mm in free-space and 157 mm when ε_r = 3.66 is considered. Thus, the ration of $\Delta z/\lambda$ is 0.033 to 0.062, indicating Δz is reasonably small as compared to the wavelength.

The propagation constant γ is expressed as

$$\gamma = \alpha + j\beta \approx j\beta, \tag{12}$$

where α is the attenuation constant that is ignored in our case, since the metamaterial shown in Figure 1 has low loss, which has been verified in our experiments shown later in this paper. The other term β is the phase constant, i.e., wave number.

For a microstrip line, the quasi-TEM (transverse electromagnetic wave) mode can be utilized [17], so when Δz is small as compared to the wavelength, the propagation constant can also be expressed as

$$\gamma = \sqrt{\frac{Z}{\Delta z}\frac{Y}{\Delta z}}. \tag{13}$$

Substituting (10), (11), and (12) into (13), the following equation is obtained:

$$\begin{aligned}\beta &= \sqrt{\left(\omega L'_R - \frac{1}{\omega C_L \Delta z}\right)\left(\omega C'_R - \frac{1}{\omega L_L \Delta z}\right)} \\ &= \frac{\sqrt{\left(\omega^2 L_R C_L - 1\right)\left(\omega^2 C_R L_L - 1\right)}}{\omega \Delta z \sqrt{L_L C_L}},\end{aligned} \tag{14}$$

where $L_R = L'_R \Delta z = 2L_p$ is the total series inductance and $C_R = C'_R \Delta z = 2C_{pg}$ is the total shunt capacitance. Other variables in (14) have the same definitions as in (10) and (11). Similarly, the characteristic impedance can be derived:

$$Z_0 = \sqrt{\frac{Z/\Delta z}{Y/\Delta z}} = \sqrt{\frac{L_L\left(\omega^2 L_R C_L - 1\right)}{C_L\left(\omega^2 C_R L_L - 1\right)}}. \tag{15}$$

Under the following designated condition,

$$\mathrm{L_R C_L = L_L C_R}, \tag{16}$$

the phase constant of (14) and the characteristic impedance of (15) are simplified, respectively:

$$\begin{aligned}\beta &= \frac{\left(\omega^2 L_R C_L - 1\right)}{\omega \Delta z \sqrt{L_L C_L}} = \frac{\left(\omega^2 L_L C_R - 1\right)}{\omega \Delta z \sqrt{L_L C_L}} \\ &= \frac{\left(\omega^2/\omega_0^2 - 1\right)\omega_L}{\omega \Delta z},\end{aligned} \tag{17}$$

$$Z_0 = \sqrt{\frac{L_L}{C_L}} = \sqrt{\frac{L_R}{C_R}}, \tag{18}$$

where

$$\omega_0 = \frac{1}{\sqrt{L_R C_L}} = \frac{1}{\sqrt{L_L C_R}}, \tag{19}$$

$$\omega_L = \frac{1}{\sqrt{C_L L_L}}. \tag{20}$$

From (17), it is seen that

$$\beta < 0 \text{ (left-handed)}, \quad \text{when } \omega < \omega_0, \tag{21}$$

$$\beta = 0, \quad \text{when } \omega = \omega_0, \tag{22}$$

$$\beta > 0 \text{ (right-handed)}, \quad \text{when } \omega > \omega_0. \tag{23}$$

2.3. Derivation of Phase and Group Velocities. The phase velocity v_p and the group velocity v_g of a TEM-mode wave or a sinusoidal wave on a transmission line are [14]

$$v_p = \frac{\omega}{\beta}, \tag{24}$$

$$v_g = \left(\frac{\partial \beta}{\partial \omega}\right)^{-1}. \tag{25}$$

Using (17), the phase and group velocities of (24) and (25) are derived:

$$v_p = \frac{\Delta z \omega_0^2 \omega^2}{\left(\omega^2 - \omega_0^2\right)\omega_L}, \tag{26}$$

$$v_g = \frac{\Delta z \omega_0^2 \omega^2}{\left(\omega^2 + \omega_0^2\right)\omega_L}. \tag{27}$$

From (26) and (27), and with relations of $\omega = \omega_L = 1/\sqrt{L_L C_L}$ for $\omega \ll \omega_0$, and $\omega = \omega_R = 1/\sqrt{L_R C_R}$ for $\omega \gg \omega_0$, the following properties are obtained:

$$v_p = -v_g = -\Delta z \omega_L = -\frac{\Delta z}{\sqrt{L_L C_L}}, \quad \text{when } \omega \ll \omega_0, \tag{28}$$

$$v_p = \propto, \quad \text{when } \omega = \omega_0, \tag{29}$$

$$v_p = v_g = \Delta z \omega_R = \frac{\Delta z}{\sqrt{L_R C_R}}, \quad \text{when } \omega \gg \omega_0, \tag{30}$$

$$v_g = \frac{\Delta z \omega_0^2}{2\omega_L}, \quad \text{when } \omega = \omega_0, \tag{31}$$

$$v_g > 0, \quad \text{when } \omega \neq 0. \tag{32}$$

The above theoretical derivations indicate that the phase velocity of a sinusoidal wave on the metamaterial shown in Figure 1 can be either negative (left-handed) or positive (right-handed), and it approaches infinity around the transition region of ω_0. However, the group velocity is always positive, no matter $\omega < \omega_0$ or $\omega > \omega_0$. This means that when $\omega < \omega_0$, the phase and group velocities on the metamaterial are antiparallel; i.e., the two vectors of v_p and v_g point to the opposite directions. However, when $\omega > \omega_0$, the phase and group velocities on the metamaterial are parallel; i.e., the two vectors of v_p and v_g point to the same direction.

2.4. Realization of Time-Space Singularity. In order to make a detailed analysis around the transition frequency, i.e., $\omega \approx \omega_0$, a linear Taylor expansion to the phase constant of (17) leads to the following simplification:

$$\beta = \beta(\omega_0) + \left.\frac{\partial\beta(\omega)}{\partial\omega}\right|_{\omega=\omega_0} \Delta\omega \approx \frac{2\omega_L}{\Delta z\omega_0^2}(\omega - \omega_0). \quad (33)$$

The phase velocity of (26) is then expressed as

$$v_p \approx \frac{\Delta z\omega_0^2}{2\omega_L(1 - \omega_0/\omega)}. \quad (34)$$

If the structure shown in Figure 1(a) is cascaded m times, as shown in Figure 1(c), the length of a broadside-coupled microstrip line is

$$l_m = m\Delta z, \quad m = 1, 2, 3 \ldots \quad (35)$$

Thus, the phase change of a sinusoidal wave propagating along a distance l_m is the following, when (33) is used.

$$\theta = \beta l_m = m\frac{2\omega_L}{\omega_0^2}(\omega - \omega_0). \quad (36)$$

Using (34) and (35), the phase delay (or ahead) time is

$$t_d = \frac{l_m}{v_p} = \frac{2m\omega_L(1 - \omega_0/\omega)}{\omega_0^2} = \frac{mf_L(1 - f_0/f)}{\pi f_0^2}. \quad (37)$$

From (36) and (37), it is seen that when $\omega = \omega_0$, both phase change θ and delay time t_d become zero, independent of m, i.e., line length. This means that the time-space reduces to a singularity from the sinusoidal wave perspective. That is, time stops and space reduces to a single point, as experienced by the propagating wave of ω_0, along any line length described by (35). As common sense, it sounds unlikely that time-space reduces to a singularity here, but this result from the theoretical analysis will later on be verified with simulations and experiments.

The group velocity on the metamaterial described by (31) has a limited value. In order to find the relation between this group velocity and the light velocity, (31) is rewritten using the expression of (19) and (20):

$$v_g = \frac{\Delta z}{2}\frac{1}{\sqrt{L_R C_R}}. \quad (38)$$

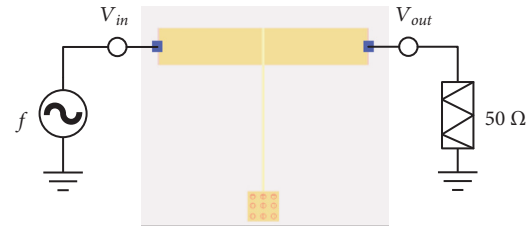

Figure 3: Illustration of time domain simulations, when a layout component ($m = 1$) is used. For $m = 2$ and 3, the layout component is cascaded twice or three times.

Under a condition of $\omega \gg \omega_0$, i.e., for right-handed traveling wave, the phase velocity is described as the following [17]:

$$v_p = \frac{1}{\sqrt{\varepsilon\mu}} = \frac{1}{\sqrt{\varepsilon_r\varepsilon_0\mu_r\mu_0}} = \frac{c_0}{\sqrt{\varepsilon_r\mu_r}} = c_{0r}, \quad (39)$$

where ε_0 and μ_0 are the permittivity and the permeability of free-space, and ε_r and μ_r are the relative permittivity and permeability in the substrate, whereas c_0 and c_{0r} are light velocities in free-space and in a medium, respectively. Comparing (39) to (30), we get the following equation:

$$\frac{\Delta z}{\sqrt{L_R C_R}} = c_{0r}. \quad (40)$$

Substituting (40) into (38), we get

$$v_g = \frac{c_{0r}}{2}. \quad (41)$$

It is seen from (41) that at the transition frequency, i.e., $\omega = \omega_0$, the group velocity is only half of the light velocity in the substrate medium, even though the phase velocity approaches infinity.

The above derivations indicate that for a TEM-mode or sinusoidal wave with a constant frequency, e.g., a single frequency carrier for communication transceivers, the singularity of time-space, i.e., vanishing of time-space, is realized when the phase velocity v_p approaches infinity at $\omega = \omega_0$. However, a deviation from this sinusoidal wave, e.g., a frequency- or phase-modulated wave, smears the singularity, as described by (36) and (37).

3. Simulation

To verify the above analytical results, simulations in both time and frequency domains are done. The simulator used is Advanced Design System (ADS) version 2017 from Keysight. Parameters listed in Table 1 are used for all simulations. The substrate material used is Rogers RO4350B with a dielectric constant $\varepsilon_r = 3.66 \pm 0.05$ and a loss factor of 0.0031 @ 2.5 GHz (0.0037 @ 10 GHz). Metal layers are Cu with a resistivity of 1.68×10^{-8} Ωm.

3.1. Time Domain. Figure 3 shows an illustration for simulations in the time domain, with a unit cell having a layout component, i.e., $m = 1$ in (35), generated from a simulation

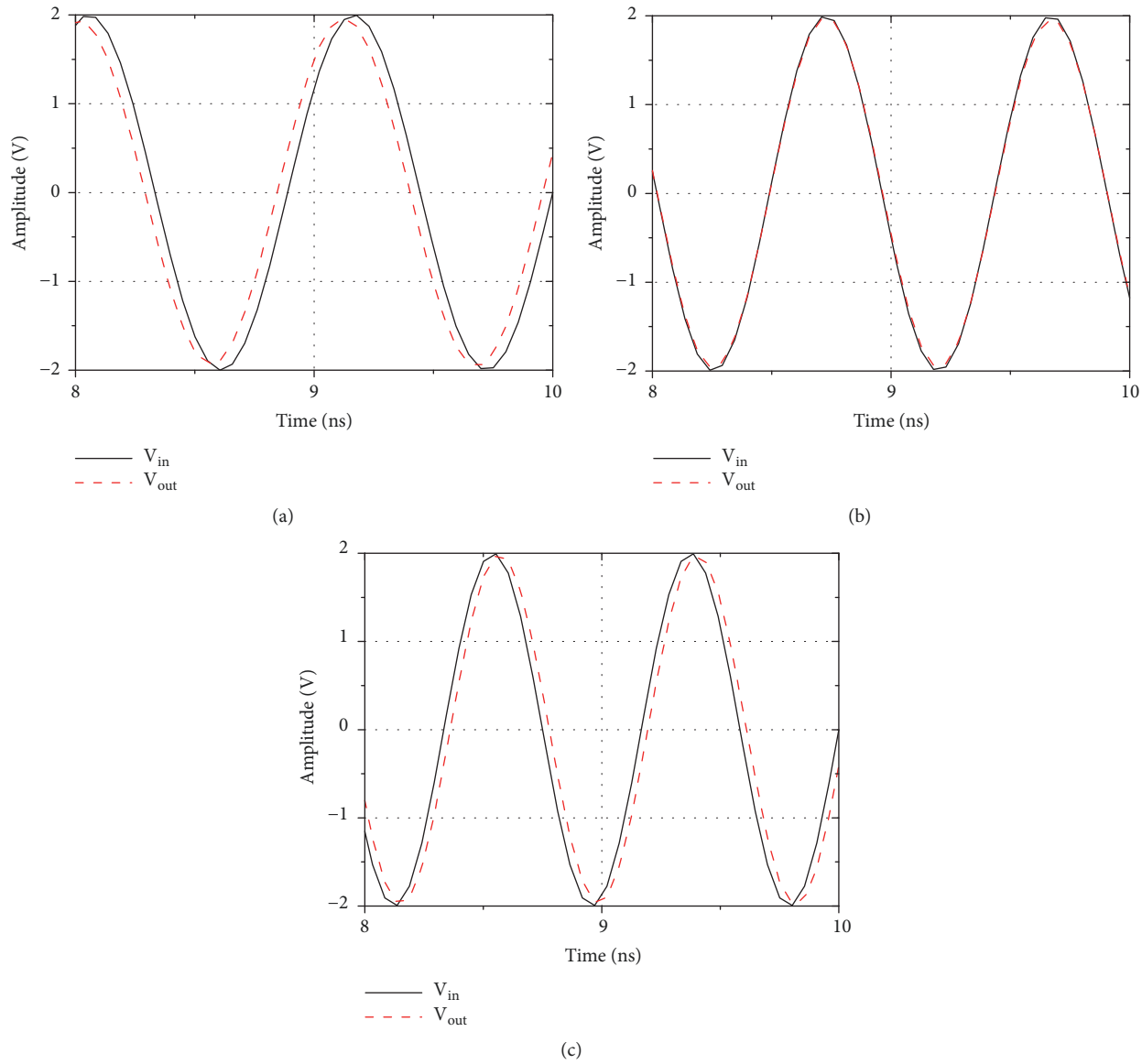

FIGURE 4: Time domain simulation when the section number $m = 1$, and the frequency of the input signal is chosen to be (a) 0.9 GHz, (b) 1.0 GHz, and (c) 1.2 GHz.

within ADS Momentum. For $m = 2$ and 3, the layout component is cascaded twice or three times (see Figure 1(c)). The source at the input generates a transient sinusoidal voltage wave. The load is a 50-Ω resistive termination.

Figure 4 shows simulation results when the frequency is chosen to be 0.9, 1.0, and 1.2 GHz, respectively. The solid line curve depicts the wave at the input, whereas the dashed line curve depicts the wave at the output. It is seen in Figure 4(a) that the dashed line curve is on the left side of the solid line curve, i.e., the phase delay time t_d is negative, indicating (see (37)) $f < f_0$, i.e., the phase velocity (see (34)) is negative. In Figure 4(b), the solid and dashed lines overlap with each other, i.e., the phase delay time t_d is zero and thus $f = f_0$ according to (37). In Figure 4(c), the dashed line curve is on the right side of the solid line curve, i.e., the phase delay time t_d is positive, indicating (see (37)) $f > f_0$, i.e., the phase velocity (see (34)) is positive.

Obviously, the results shown in Figures 4(a) and 4(b) are abnormal as compared to those from a conventional microstrip line. On the one hand, one may argue that this can happen if the output curve is one period (360°) after the input curve on a conventional microstrip line. The fact is that the unit cell ($m = 1$) used in Figure 3 has a length of 9.80 mm (see Table 1) that is much shorter than the wavelength (300 mm in free-space and 157 mm when $\varepsilon_r = 3.66$ is considered) at 1 GHz, so this argument cannot be true. On the other hand, the negative or zero phase delay time agrees very well with the formula shown in (37), when $f \leq f_0$. When $f > f_0$, the phase delay time shown in (37) is positive as shown in Figure 4(c), which is similar to that from a conventional microstrip line.

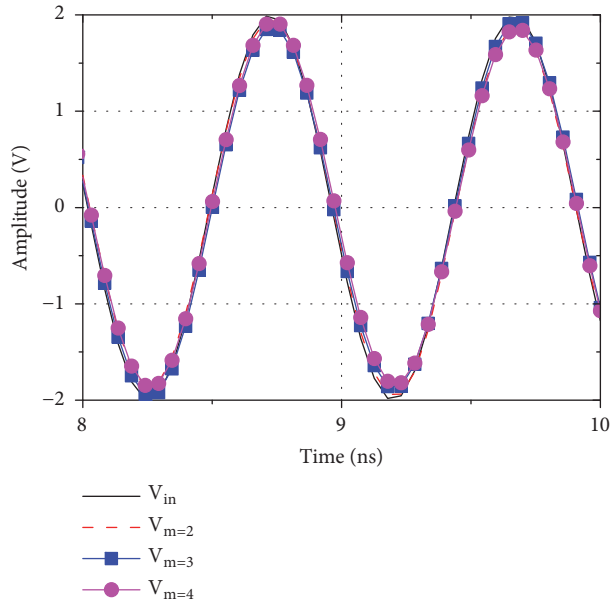

FIGURE 5: Time domain simulation of cascaded sections at 1 GHz, when m = 2, 3, and 4, respectively.

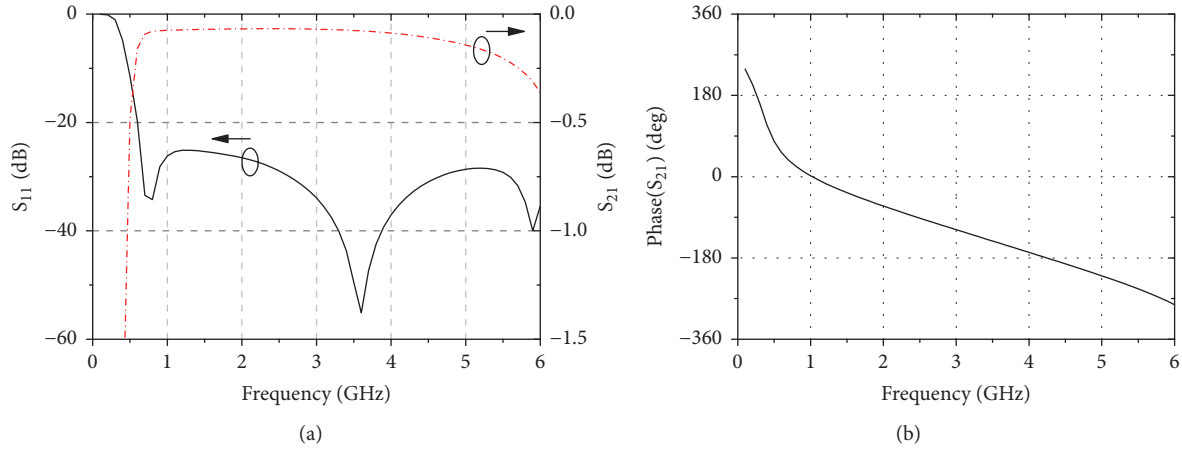

FIGURE 6: Simulation of S-parameters when m = 1: (a) S_{21} and S_{11} magnitudes (dB), and (b) S_{21} phase response; zero phase delay at 1 GHz is seen.

Figure 5 depicts simulation results when the frequency is chosen to be $f = f_0 = 1$ GHz, and the layout component shown in Figure 3 is cascaded such that m (see (35)) is chosen to be 2, 3, and 4, respectively. It is seen that all output curves overlap with the input curve, similar to that in Figure 4(b). Similar to the explanation for Figure 4(b), the overlap of the input and output curves in Figure 5 cannot be interpreted with repeated wave periods when m = 2, 3, and 4, since the line lengths, i.e., l_m = 19.6, 29.4, and 39.2 mm, are still much shorter than a wavelength of 300 mm in free-space or 157 mm in the substrate with a relative permittivity of $\varepsilon_r = 3.66$.

Simulation results similar to Figure 4(b) were also observed, when m is chosen to be 3 and f_0 = 2 and 3 GHz, respectively. Obviously, zero phase delay time, i.e., $t_d = 0$, has been realized at all the designated frequencies of 1, 2, and 3 GHz, which is independent of line length, when it is chosen to be $m\Delta z$, according to (35).

3.2. Frequency Domain. Due to symmetry of the line structure (see Figure 1), only scatter parameters of S11 and S21 are presented in the paper. Figure 6 depicts simulation results, when the layout component used is the same as that in Figure 4. At 0.9, 1.0, and 1.2 GHz, the S21 phase is +11.53°, 0°, and -14.67°, respectively. Low loss is observed in the S21 and S11 amplitude curves up to 4 GHz in Figure 6(a). Moreover, the transition point, from positive to negative phase when $f = f_0 = 1$ GHz, is clearly seen on the S21 phase curve in Figure 6(b).

Figure 7 depicts an S21 diagram using the same structure as that in Figure 6, but m is chosen to be 2 and 3, respectively. Again, low loss up to 4 GHz is observed in Figure 7(a), and it is also seen in Figure 7(b) that the transition point, from positive to negative S21 phase at $f = f_0 = 1$ GHz, remains the same, even though the tangents of the phase curves have changed.

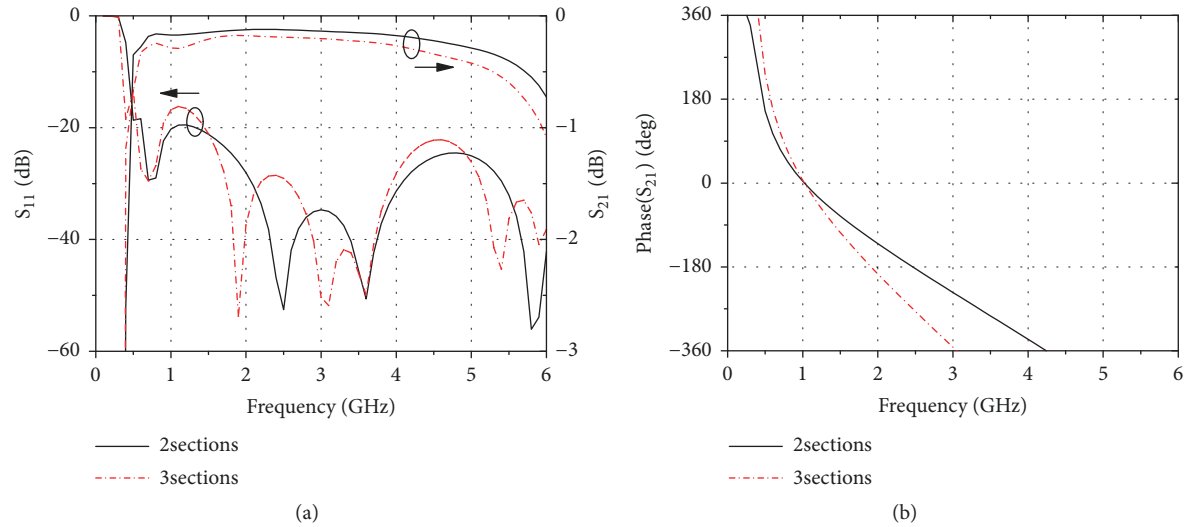

FIGURE 7: Simulation of S-parameters, $f = f_0 = 1$ GHz, and $m = 2$ and 3, respectively: (a) S_{11} and S_{21} magnitudes (dB), and (b) S_{21} phase response.

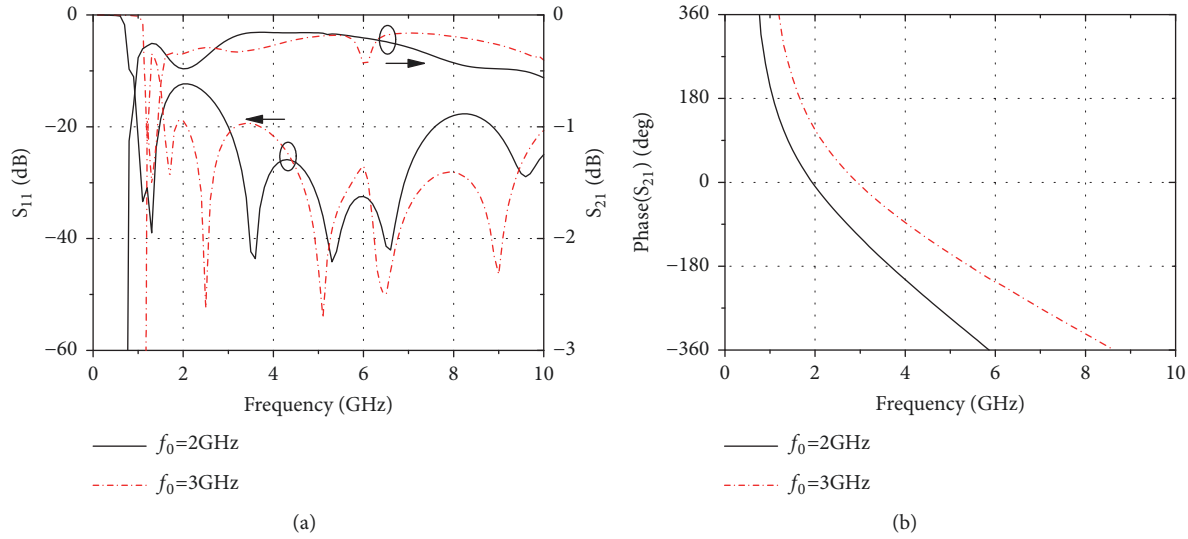

FIGURE 8: Simulation of S-parameters, $m = 1$: (a) S_{11} and S_{21} magnitudes (dB), and (b) S_{21} phase response.

Figure 8 depicts an S21 diagram like that in Figure 6, but $f_0 = 2$ and 3 GHz, respectively. Similar properties of low loss and zero phase delays are observed, as compared to the case at $f_0 = 1$ GHz.

Figure 9 depicts an S21 diagram like that in Figure 6, but $m = 10$, 20 and 30, respectively. That is, the line length is 1.14 λ, 2.29 λ, and 3.44 λ, respectively, where λ is the wavelength at 1 GHz. It is seen in Figure 9(b) that the zero phase delay remains at $f_0 = 1$ GHz, even though the line length has changed such that it is random with respect to the wavelength.

4. Experiment

For verification purposes, experimental samples were designed and fabricated in our printed circuit laboratory at Linköping University. Measurements in the time domain were done in our test and measurement laboratory with an oscilloscope WaveMaster/SDA/DDA 8 Zi-B from LeCroy, whereas measurements in the frequency domain were done with a vector network analyzer ZVM 20 GHz from Rohde & Schwarz.

4.1. Sample Design and Fabrication. Samples with the structure shown in Figure 1 and dimension parameters listed in Table 1 have been designed and fabricated. Figure 10 shows a photo of the fabricated samples, at $f_0 = 1$, 2, and 3 GHz, respectively.

4.2. Time Domain Measurement. Figure 11 shows that the measurement result corresponds to Figure 4(b). Other measurement results similar to simulation results shown in

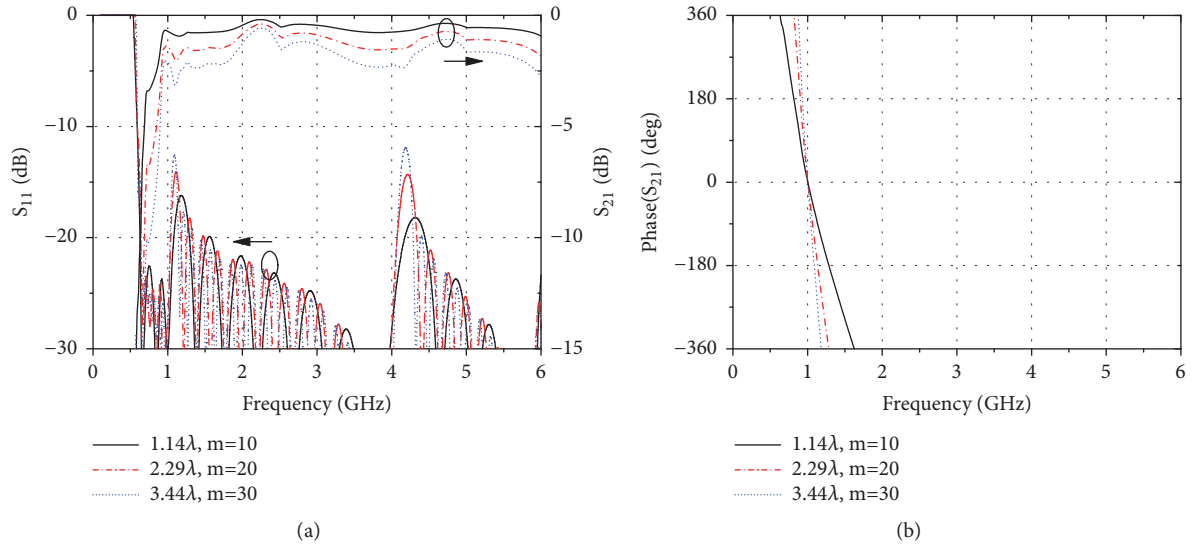

FIGURE 9: Simulation of S-parameters, m = 10, 20, and 30, respectively: (a) S_{11} and S_{21} magnitudes (dB), and (b) S_{21} phase response.

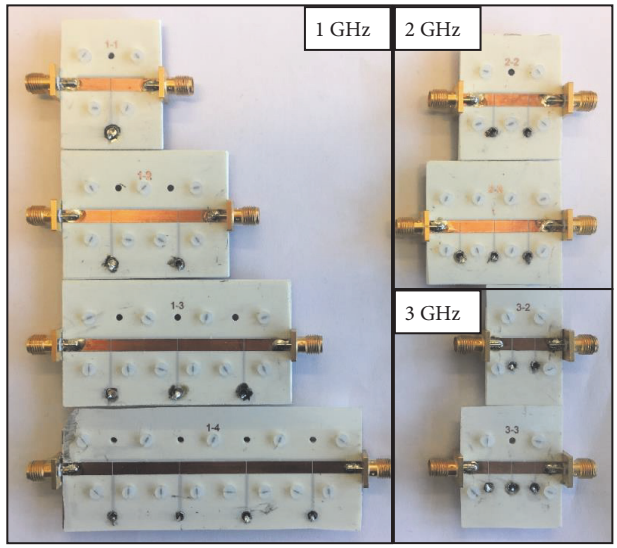

FIGURE 10: Photo of fabricated samples.

Figures 4(a) and 4(c), as well as in Figure 5, are all observed with the samples shown in Figure 10.

4.3. Frequency Domain Measurement. Figure 12 shows an S21 diagram using the same structure as that in Figure 7. It is seen that at the transition point of f_0 = 1 GHz, zero phase delay is realized, when the section number m = 2 and 3, respectively. Figure 13 depicts S-parameter diagrams like that in Figure 12, but f_0 = 2 and 3 GHz, respectively. By comparing Figure 12 with Figure 7, and Figure 13 with Figure 8, it is apparent that the simulation and experiment results agree well with each other. The larger loss from experimental samples shown in Figures 12 and 13 as compared to those in Figures 7 and 8 is due to discontinuities from SMA connectors and some misalignment of metal layers when processing experimental samples in our lab.

5. Results and Discussion

Both the simulation and experimental results have verified that the phase velocity of a sinusoidal wave can approach infinity at a designated angular frequency ω_0 on a broadside-coupled transmission line with short-circuit stubs, as theoretically described by (26) and (29). However, according to (31) the group velocity has still a limited value, i.e., half of the light velocity according to (41), indicating that the group velocity can never exceed the light velocity ($c_0 = 3 \times 10^8$ m/s in free-space), even though the phase velocity can approach infinity.

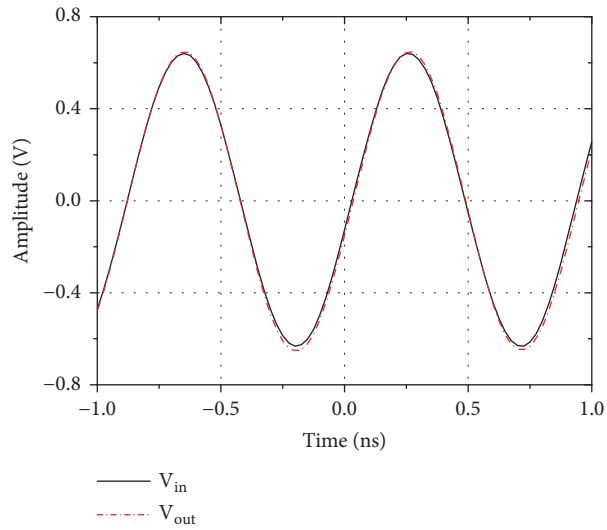

Figure 11: Time domain measurement when $m = 1$, and the frequency of the input signal is chosen to be 1.0 GHz.

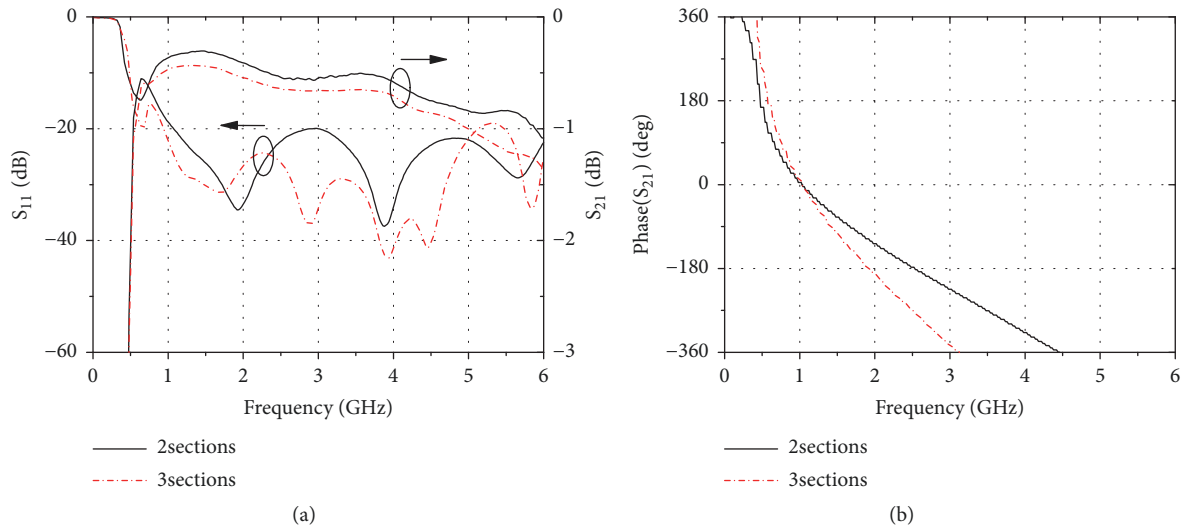

Figure 12: Measurement of S-parameters, $f_0 = 1$ GHz, and $m = 2$ and 3, respectively: (a) S_{11} and S_{21} magnitudes (dB), and (b) S_{21} phase response.

5.1. Realization of Zero Permittivity and Permeability. Equation (29) can be rewritten as

$$v_p = \frac{1}{\sqrt{\varepsilon_{\omega_0}\mu_{\omega_0}}} = \propto, \quad \text{when } \omega = \omega_0, \tag{42}$$

where ε_{ω_0} and μ_{ω_0} are permittivity and permeability of the metamaterial shown in Figure 1, at a designated frequency of ω_0. From (42), we still cannot answer the question as to whether we have realized both zero permittivity and zero permeability, or only one of them. However, from (10) and (11) we have

$$\begin{aligned} Z &= j\left(\omega_0 L_R' \triangle z - \frac{1}{\omega_0 C_L}\right) = j\left(\omega_0 L_R - \frac{1}{\omega_0 C_L}\right) \\ &= j\omega_0 m' \mu_{\omega_0} \end{aligned} \tag{43}$$

$$\begin{aligned} Y &= j\left(\omega_0 C_R' \triangle z - \frac{1}{\omega_0 L_L}\right) = j\left(\omega_0 C_R - \frac{1}{\omega_0 L_L}\right) \\ &= j\omega_0 n' \varepsilon_{\omega_0} \end{aligned} \tag{44}$$

where m' and n' are two nonzero constants, and $m'\mu_{\omega_0}$ and $n'\varepsilon_{\omega_0}$ are equivalent inductance and capacitance of the metamaterial, respectively. Inserting (19) into (43) and (44), we obtain $Z = 0$ and $Y = 0$, and thus $\mu_{\omega_0} = 0$ and $\varepsilon_{\omega_0} = 0$, respectively. Thus, we can conclude that both zero permittivity and zero permeability are realized when the phase velocity approaches infinity at the designated angular frequency ω_0 of the metamaterial of any length according to (35).

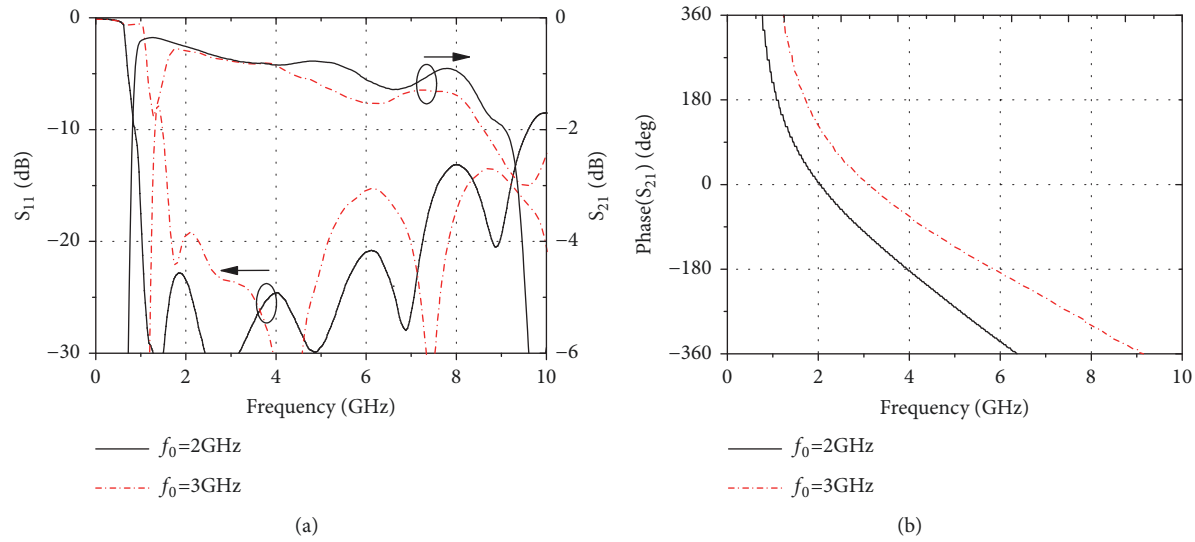

FIGURE 13: Measurement of S-parameters, $m = 1$: (a) S_{11} and S_{21} magnitudes (dB), and (b) S_{21} phase response.

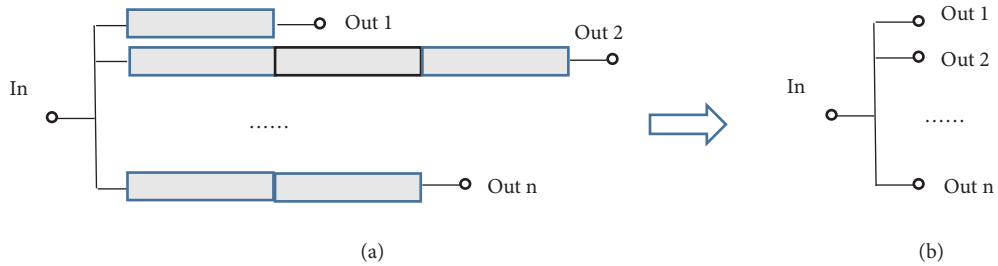

FIGURE 14: Illustration of time-space reduces to a singularity of the metamaterial shown in Figure 1(a): (a) the unit cell is connected in both series and parallel; (b) its equivalent circuit where the input and output ports merge to the singularity around the designated frequency where the phase velocity approaches infinity.

5.2. Traveling Wave or Standing Wave. One probable doubt can be that the observed time-space singularity at a designated frequency in this study is just standing waves between the input and output ports such that the phase difference is zero between the two ports. However, the simulated S21 curves in Figures 6(a), 7(a), and 8(a) and the measured S21 curves in Figures 12(a) and 13(a) have clearly shown traveling wave properties, no matter how the section numbers or frequencies are changed. Moreover, as shown in Figure 9, when the line length is randomly changed with respect to the wavelength λ, the zero phase delay remains at the designated frequency f_0. All those results also support the analytical results of (34)-(37) derived for a traveling wave, not a standing wave between the input and output ports.

5.3. Bandwidth and Application in Microwave Design. This study has started from the first principle of Maxwell's equations and the transmission line theory. The only two approximations made are, first, the minimum unit cell length Δz that is not infinitesimally small in (10) and (11) and, second, the Taylor expansion of (33). Thus, the analytical results should provide fundamental insights. For instance, the correctness of (34)-(37) has been verified with both simulation and experimental results. One of the remaining questions is that regarding the bandwidth of the metamaterial at a designated frequency f_0 when both permittivity and permeability are near zero. This can be analyzed further with (34), (36), and (37). As seen in Figures 12(b) and 13(b), we have a rather smooth positive to negative phase transition around f_0. Therefore, a certain bandwidth can be utilized, in which both permittivity and permeability are near zero, but not exactly zero.

With a near-zero permittivity and permeability realized with the presented low loss metamaterial, microwave designs can be simplified. According to (8) and (9), Kirchhoff's current and voltage laws are still valid at a microwave or mm-wave frequency, when circuitries are designed with the metamaterial around that frequency. As illustrated in Figure 14, no matter how the unit cell shown in Figure 1(a) is connected in series or parallel, the input and output ports merge to a singularity at the designated frequency where the phase velocity approaches infinity. This means that the microwave design methodology in terms of impedance matching, utilization of Smith Chart, and consideration of phase delay is not needed. Instead, the design methodology for analog circuits in terms of voltage loop and current

divergence can be used directly. Moreover, some new circuit topology with zero phase delay of interconnects of arbitrary lengths can be worked out.

5.4. Phase, Group, and Propagation Velocities. It is commonly understood that in a homogenous and right-handed material, a harmonic electromagnetic wave propagates with a phase velocity, but a modulated wave from a harmonic electromagnetic wave propagates with a group velocity. However, one must notice that phase, group, and propagation velocities are different concepts; the propagation velocity of a wave can be different from either a phase or a group velocity.

This study has shown that a phase velocity on our presented metamaterial can approach infinity at a designated frequency of f_0, but the group velocity is only half of the light velocity in the same substrate of the metamaterial. This result agrees well with that from an electromagnetic field study [8], in which the author shows that a dispersive wave front propagates in the metamaterial, in the beginning, with a group velocity that is half of the propagation, i.e., light velocity in free-space; see Figure 4 of [8]. However, at late times when a steady state is reached the incoming and outcoming waves are "in lockstep with each other", resulting in an infinitively large propagation velocity, i.e., near-zero delay, through the metamaterial; see Figure 5 of [8].

Within a small bandwidth Δf around f_0, a phase velocity on our presented metamaterial still approaches infinity. Thus, narrowband signals, e.g., a frequency-modulated signal with a bandwidth of Δf around f_0 or a phase-modulated signal of f_0, can be transferred with near-zero time delay between the input and output ports, according to the principle illustrated in Figure 14, even though the group velocity on the metamaterial before reaching a steady state is only half of the light velocity in the substrate. This is simply due to the fact that the group velocity according to (41) describes the speed of wave dispersion fronts before they reach the output ports shown in Figure 14. After reaching an output port, the input wave of f_0 propagates through the metamaterial with a phase velocity approaching infinity.

6. Conclusion

Using our invented low loss metamaterial of broadside-coupled transmission lines with short-circuit stubs, it is shown that a phase velocity of a traveling sinusoidal wave can approach infinity at various designated frequencies, resulting in zero permittivity and zero permeability. This means that the traveling sinusoidal wave experiences time stop and space shrink to a singularity, independent of its size. This property has been derived from theory, analyzed with simulation, and verified with experimental results.

With this low loss metamaterial, the traditional microwave theory and techniques can be simplified for narrowband signals around various designated frequencies where the phase delay is near zero. That is, the traditional electrical circuit theory based on Kirchhoff's laws is still valid in the microwave or mm-wave spectrum for narrowband signals, utilizing a low loss metamaterial. Consequently, the microwave design methodology in terms of impedance matching, utilization of Smith Chart, and consideration of phase delay is not needed. Instead, the design methodology for analog circuits in terms of voltage loop and current divergence can be used directly. Moreover, some new circuit topology with zero phase delay of interconnects of arbitrary lengths can be worked out.

Data Availability

The simulation and experimental data used to support the findings of this study are included within the article.

Conflicts of Interest

The authors declare that there are no conflicts of interest regarding the publication of this paper.

Acknowledgments

The authors thank Gustav Knutsson at Linköping University for fabrication of experimental samples. This work has been financially supported by the Faculty of Science and Engineering at Linköping University, Sweden. The second author also acknowledges the support by the China Scholarship Council (File No. 201706075057).

References

[1] S. Gong and M. Karlsson, "Pushing the wireless data rate to the internet speed," *IEEE Access*, vol. 4, pp. 8787–8792, 2016.

[2] D. R. Smith, W. J. Padilla, D. C. Vier, S. C. Nemat-Nasser, and S. Schultz, "Composite medium with simultaneously negative permeability and permittivity," *Physical Review Letters*, vol. 84, no. 18, pp. 4184–4187, 2000.

[3] R. A. Shelby, D. R. Smith, S. C. Nemat-Nasser, and S. Schultz, "Microwave transmission through a two-dimensional, isotropic, left-handed metamaterial," *Applied Physics Letters*, vol. 78, no. 4, pp. 489–491, 2001.

[4] A. Lai, C. Caloz, and T. Itoh, "Composite right/left-handed transmission line metamaterials," *IEEE Microwave Magazine*, vol. 5, no. 3, pp. 34–50, 2004.

[5] V. G. Veselago, "The electrodynamics of substances with simultaneously negative values of ε and μ," *Soviet Physics Uspekhi*, vol. 10, no. 4, pp. 509–514, 1968.

[6] G. V. Eleftheriades, A. K. Iyer, and P. C. Kremer, "Planar negative refractive index media using periodically L-C loaded transmission lines," *IEEE Transactions on Microwave Theory and Techniques*, vol. 50, no. 12, pp. 2702–2712, 2002.

[7] C. Caloz and T. Itoh, "Transmission line approach of left-handed (LH) materials and microstrip implementation of an artificial LH transmission line," *IEEE Transactions on Antennas and Propagation*, vol. 52, no. 5, pp. 1159–1166, 2004.

[8] R. W. Ziolkowski, "Propagation in and scattering from a matched metamaterial having a zero index of refraction," *Physical Review E: Statistical, Nonlinear, and Soft Matter Physics*, vol. 70, no. 4, Article ID 046608, 2004.

[9] D. Eliecer, X. Cheng, and Y. Yoon, "Highly compact surface micromachined metamaterial circuits using multilayers of low-loss Benzocyclobutene for microwave and millimeter wave applications," in *Proceedings of the 2012 IEEE 62nd Electronic*

Components and Technology Conference (ECTC), pp. 2062–2069, San Diego, CA, USA, May 2012.

[10] A. Rennings, T. Liebig, C. Caloz, and P. Waldow, "MIM CRLH series mode zeroth order resonant antenna (ZORA) implemented in LTCC technology," in *Proceedings of the 2007 Asia-Pacific Microwave Conference (APMC '07)*, pp. 1–4, Bangkok, Thailand, December 2007.

[11] Y. Horii, "Development of LTCC-based super-compact multilayered CRLH transmission lines and broadband applications," in *Proceedings of the 2012 Asia-Pacific Symposium on Electromagnetic Compatibility (APEMC)*, pp. 149–152, Singapore, May 2012.

[12] A. M. Mahmoud and N. Engheta, "Wave-matter interactions in epsilon-and-mu-near-zero structures," *Nature Communications*, vol. 5, pp. 1–7, 2014.

[13] D. Schuette, I. Irfanullah, S. Nariyal, S. Khattak, and B. D. Braaten, "Strong coupling (crosstalk) between printed microstrip and complementary split ring resonator (CSRR) loaded transmission lines in multilayer printed circuit boards (pcb)," in *Proceedings of the 2016 IEEE International Conference on Electro Information Technology (EIT)*, pp. 0196–0199, Grand Forks, ND, USA, May 2016.

[14] D. M. Pozar, *Microwave Engineering*, Wiley, 3rd edition, ISBN 0-471-44878-8, pp. 6-9, 151-154, 682-683, 2005.

[15] M. Karlsson and S. Gong, "Circular dipole antenna for mode 1 UWB radio with integrated balun utilizing a flex-rigid structure," *IEEE Transactions on Antennas Propagation*, vol. 57, no. 10, pp. 2967–2971, 2009.

[16] M. Karlsson, P. Hakansson, and S. Gong, "A frequency triplexer for ultra-wideband systems utilizing combined broadside- and edge-coupled filters," *IEEE Transactions on Advanced Packaging*, vol. 31, no. 4, pp. 794–801, 2008.

[17] R. Ludwig and P. Bretchko, *RF Circuit Design: Theory and Applications*, Prentice-Hall, Inc., 2nd edition, 2009.